

# The role of oxygenic groups and $sp^3$ carbon hybridization in activated graphite electrodes for vanadium redox flow batteries

*Ali Hassan*<sup>a,b,c</sup>, *Asnake Sahele Haile*<sup>d</sup>, *Theodore Tzedakis*<sup>a</sup>, *Heine Anton Hansen*<sup>b</sup>, *Piotr de Silva*<sup>b\*</sup>

<sup>a</sup> Laboratoire de Génie Chimique, UMR CNRS 5503, Université de Toulouse, UT-III-Paul Sabatier, 118 Route de Narbonne, F-31062 Toulouse, France.

<sup>b</sup> Department of Energy Conversion and Storage, Technical University of Denmark, 2800 Kgs. Lyngby, Denmark

<sup>c</sup> Chemical Engineering Department, MNS University of Engineering and Technology, Multan, Pakistan

<sup>d</sup> Center for Environmental Science, College of Natural and Computational Sciences, Addis Ababa University, Ethiopia

\*e-mail: pdes@dtu.dk

**Abstract:** Graphite felt is a widely used electrode material for vanadium redox flow batteries. Electrode activation leads to the functionalization of the graphite surface with epoxy, OH, C=O, and COOH oxygenic groups and changes the carbon surface morphology and electronic structure; thus, improving the electrode's electroactivity relative to the untreated graphite. In this study, we conduct density functional theory (DFT) calculations to evaluate functionalization's role towards the positive half-cell reaction of the vanadium redox flow battery. The DFT calculations show that oxygenic groups improve the graphite felt's affinity towards the  $VO^{2+}/VO_2^+$  redox couple in the following order: C=O > COOH > OH > basal plane. Projected density of states (PDOS) calculations show that these groups increase the electrode's  $sp^3$  hybridization in the same order. We conclude that the increase in the  $sp^3$  hybridization is responsible for the improved electroactivity, while the oxygenic groups' presence is responsible for this  $sp^3$  increment. These insights can help in the better selection of activation processes and optimization of their parameters.

**Keywords:** Vanadium redox flow battery, graphite electrode, electrode activation, density functional theory, carbon.

## 1. Introduction

Due to the environmental challenges, the share of power production from renewable sources is increasing rapidly. There is a growing interest in redox flow batteries for better energy management of these resources' intermittent nature. The fundamental aspect of redox flow batteries is their detached power and energy density that distinguishes them from conventional batteries. Energy is stored in the electroactive material dissolved in the electrolyte and stored in tanks outside of the stack. The energy density is solely depending upon the amount of the electroactive material [1]. Therefore, flow batteries can be easily aligned with the energy demand by changing the electrolyte volume and the storage installation [2].

Vanadium redox flow batteries (VRFB) successfully made up to the commercial level, but they still suffer from relatively low power density. The power density of VRFBs depends upon the stack, and its optimization is essential to improve the overall efficiency and reduce the cost [3]. The system's kinetic reversibility depends on the electrodes, as the positive and negative half-cell reactions occur at the electrode-electrolyte interface. Besides, the available surface area of the electrode is also linked to energy and current efficiency. So, the selection of the electrode material is crucial for stack optimization. [4]. The graphite felts are a suitable choice for flow battery electrodes due to their fibrous structure and high available surface area. Moreover, these felts are inexpensive and stable in the acidic condition of the VRFBs (2 M-5 M acids); however, they show low kinetic reversibility against the vanadium redox couples and exhibit hydrophobic behavior. [5,6]

The kinetics of the positive half-cell reaction is slow compared to the negative half-cell, so the rate limitation is coming from the former [7,8]. Chemical, thermal, and electrochemical oxidative

treatment is widely investigated to improve the graphite felts' electroactivity [9–11]. These oxidative approaches fabricate different oxygenic groups (epoxy, OH, COOH, C=O) on the electrodes and increase the  $sp^3$  hybridization of the carbon atoms in the material. Their proportions depend on the nature and extent of the oxidative activation process [12]. Some activation procedures lead to the fabrication of higher OH concentration [10,13] while other inscribe more C=O and COOH groups [14]. The common aspect of all the activation procedures is inducing structural changes in the felt, which result in the increased  $sp^3$  carbon hybridization in the electrode. This activation is believed to provide more reaction sites for the redox processes in the vanadium flow battery.

Because of the simultaneous presence of all these individual groups (epoxy, OH, COOH, C=O,  $sp^3$  hybridization) in the electrode, it is difficult to experimentally distinguish these components' individual roles in the catalysis of the vanadium redox reaction [15]. Consequently, there are many different experimental hypotheses about the role of oxygenic groups. Z. He et al. suggested that COOH groups are acting as catalytic sites [9]. Li et al. proposed that the COOH groups improve the reaction rate, while the C-OH and C=O impede the reactions [16]. Skyllas-Kazacos hypothesized that C-OH groups are the active sites for the reaction [17]. On the contrary, some other reports suggest the impeding role of oxygenic groups towards positive half-cell reaction and indicate that the electrode's structure is the predominant factor. [15,18]. Lie et al. proposed that the oxygenic groups are the sole reason for the catalysis, and surface area is not playing any significant role [19]. Computational methods such as molecular dynamics and electronic structure calculations can provide theoretical insight into such experimentally complicated situations. [20–23]

In this study, the density functional theory (DFT) calculations are performed to evaluate the individual roles of epoxy, OH, C=O, COOH, and surface morphological changes in the  $\text{VO}^{2+}/\text{VO}_2^+$  redox reaction. The correlation between the surface morphology and oxygenic groups is also established using the projected density of state calculations (PDOS). The study shows that the increase in the  $\text{sp}^3$  hybridization during the activation process is directly related to the catalysis of the  $\text{VO}^{2+}/\text{VO}_2^+$  reaction. The oxygenic groups are in turn responsible for the increase of the  $\text{sp}^3$  hybridization in the electrode.

## **2. Methods**

We performed DFT calculations using the GPAW program [24]. All the calculations are based on the projector augmented wave (PAW) method [25,26]. The structures are built and visualized using the “Atomic Simulation Environment” (ASE) package [27]. A plane-wave cut-off energy of 400 eV is used in the calculations, sufficient to converge the water splitting on the graphene layer reaction energy (supplementary data S. 1). A  $5 \times 5 \times 1$  mesh of k-points is chosen for all the calculations on the carbon felt model, as the system started converging from this point (supplementary data S. 1). Bayesian error estimation functional with van der Waals correlation (BEEF-vdW) is used as the exchange-correlation functional [28]. The 40 Å vacuum is provided in the z-axis direction, while the periodic boundary conditions are applied in the  $x$  and  $y$  directions.

## **3. Results and discussion**

One layer of graphite (pristine- 0 0 0 1) is modelled as an initial reference structure. It is assumed computationally equivalent to the untreated graphite felt. The graphene layer is based on the relaxed C-C bond length of 1.4215 Å (supplementary data S. 2). To avoid any interactions in the

$x$  and  $y$  directions due to periodicity, 50 carbon atoms are included in the surface model (supplementary data S. 3).

All the oxidative activation processes described in the literature are carried out either at very high temperatures (400 °C- 1000 °C) or under intense chemical conditions for a long time (~ 10-15 h), Such processing creates defects at the surfaces and edges [10,26,27], which are likely covered with functional groups upon further oxidation. [6,16,32]. At high temperature and longer duration, the defect of six-carbon (6C) ring is the most stable defect in the basal surface of graphite [33]. The purpose of this study is to investigate the interaction of the  $\text{VO}^{2+}/\text{VO}_2^+$  with the epoxy, OH, C=O, and COOH groups; and to establish possible correlations between structural changes,  $\text{sp}^2/\text{sp}^3$  hybridization, oxygenic groups, and the  $\text{VO}^{2+}/\text{VO}_2^+$  affinity to the electrode. To this end, the following model structures are considered.

a) Single layer of the basal surface of the graphite (BG) - Fig 1a

b) Hydroxyl group on the basal surface (BG-OH)- Fig 1b

c) Epoxy group on the basal surface (BG-O)- Fig 1c

d) Basal surface with a 6C defect and all dangling bonds saturated with hydrogen atoms [29].

This model is used to study the C-H kinetics against the positive half-cell reaction. (BG-D-H)

Fig 1d.

e) Basal surface with a 6C defect and only five dangling bonds saturated with hydrogen atoms.

This model is used to study the interactions between the basal defect with the vanadium ions.

(BG-D) fig 1e.

f) Basal surface with a 6C defect with five dangling bonds saturated with hydrogens and one with a C=O, C-OH or -COOH group (BG-D-OH, BG-D=O, BG-D-COOH) - Fig 1f, g, h

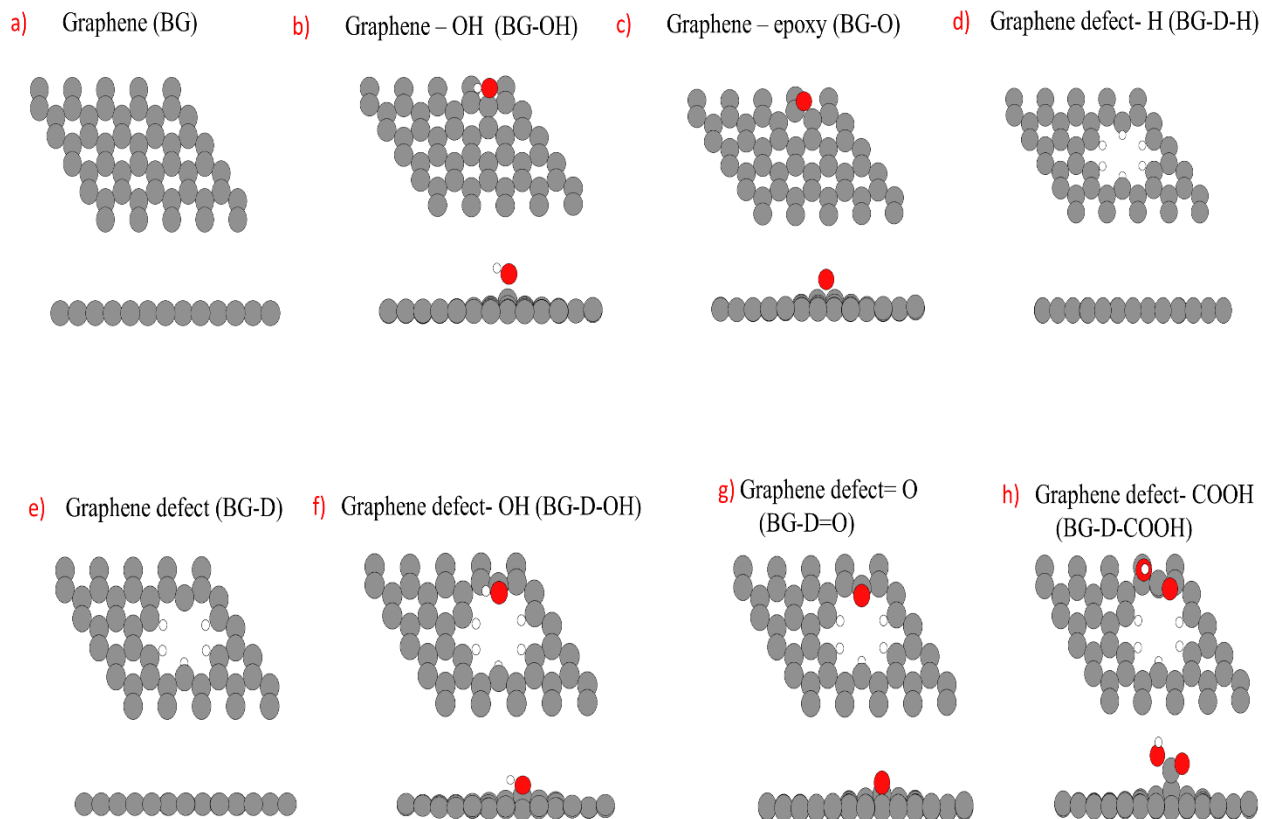


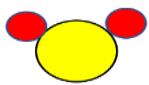
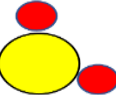
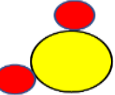
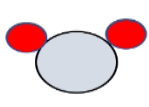
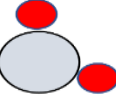
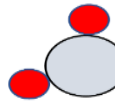
**Fig 1** Relaxed structures of a) basal surface (BG) b) basal surface with a hydroxyl group (BG-OH), c) basal surface with epoxy group (BG-O), d) basal defect saturated with hydrogen (BG-D-H), e) basal defect (BG-D), f) basal defect saturated with a hydroxyl group (BG-D-OH), g) basal defect saturated with a carbonyl group (BG-D=O), h) basal defect saturated with a carboxyl group (BG-D-COOH).

The affinity of the  $\text{VO}^{2+}/\text{VO}_2^+$  redox couple to the electrode surface is studied in vacuum to avoid any solvent interference. As the solvent interactions are also important at the electrode-electrolyte interface, the study of the water interactions with all the representative surfaces is done separately, although we expect trends in the interaction between the  $\text{VO}^{2+}/\text{VO}_2^+$  redox couple and the electrode surfaces to be independent of the solvent. The adsorption energies can

provide insights into the reactant species' interactions with the electrode surface and can be related to the kinetics of the reaction [34–36]. So, in this study, adsorption energies of  $V^{(IV)}$ ,  $V^{(V)}$ , and  $H_2O$  are determined on the surfaces of graphite felt (GF) using the following equation.

$$E_{(adsorption)} = E_{(surface+adsorbate)} - E_{(surface)} - E_{(adsorbate)} , \quad (1)$$

where  $E_{(adsorption)}$  is the adsorption energy,  $E_{(surface+adsorbate)}$  and  $E_{(surface)}$  are the energies of surfaces with and without adsorbate respectively, and  $E_{(adsorbate)}$  is the total energy of the adsorbate molecule. To find the adsorbate's optimal binding to the surface, different initial orientations of  $VO^{2+}$ ,  $VO_2^+$ , and  $H_2O$  are considered for further optimization (fig. 2).

	Orientation-1	Orientation-2	Orientation-3	Orientation-4	Orientation-5	Orientation-6
$VO^{2+}$						
$VO_2^+$						
$H_2O$						

**Fig 2** Different initial orientations of the  $VO^{2+}$ ,  $VO_2^+$ , and  $H_2O$  adsorbates relative to the graphite plane located at the bottom ( $xy$  plane).

### 3.1 Interaction of the $V(IV)$ with activated electrode surfaces

The interaction of the  $VO^{2+}$  with modified electrode surfaces (fig. 1) is studied in this section. For that, the  $VO^{2+}$  ion is initially placed 2.5 Å above the modified surfaces. Adsorption energies are calculated by equation 1 for each of the six initial orientations of the adsorbate. The structure with the maximum adsorption energy is the most thermodynamically stable

	BG (eV)	BG -OH (eV)	BG-epoxy (eV)	BG-D-H (eV)	BG-D (eV)	BG-D-OH (eV)	BG-D-O (eV)	BG-D-COOH (eV)
Orientation 1	-0.599	Unstable OH	Unstable OH	-1.758	-2.174	-1.35	-2.154	-1.633
Orientation 2	-0.155			-1.716	-3.273	-0.235	0.02	-
Orientation 3	-1.31			-1.723	-3.164	-0.945	-2.171	-
Orientation 4	-1.312			-1.724	-3.165	-1.293	-2.688	-2.538
Orientation 5	-1.311			-1.724	-3.199	-1.328	-2.171	-
Orientation 6	-1.317			-1.724	-3.226	-0.309	-2.696	-1.715
<b>Most stable</b>	<b>-1.317</b>			<b>-1.758</b>	<b>-3.273</b>	<b>-1.35</b>	<b>-2.696</b>	<b>-2.538</b>

**Table 1** Adsorption energies (eV) of the  $\text{VO}^{2+}$  at different representative geometries

All the most stable relaxed structures of adsorbed  $\text{VO}^{2+}$  are shown in fig. 3.

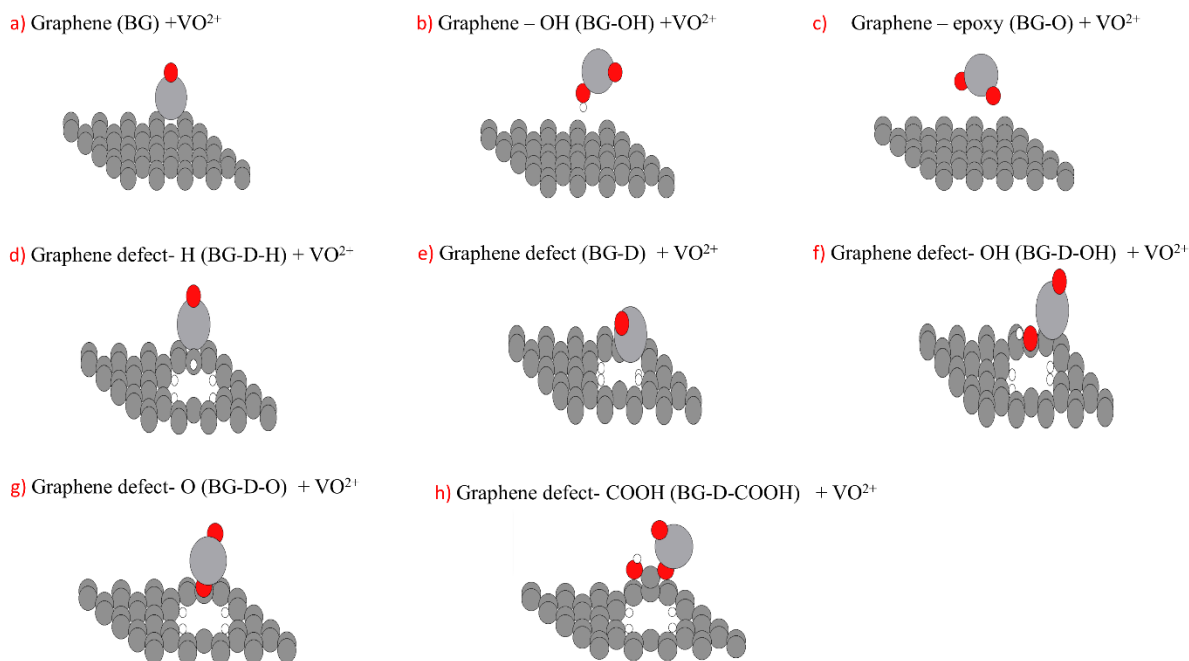


**Fig. 3** Relaxed structures of  $\text{VO}^{2+}$  adsorbed on a) basal surface (BG) b) basal surface with a hydroxyl group (BG-OH), c) basal surface with epoxy group (BG-O), d) basal defect saturated with hydrogen (BG-D-H), e) basal defect (BG-D), f) basal defect saturated with a hydroxyl group (BG-D-OH), g) basal defect saturated with a carbonyl group (BG-D-O), h) basal defect saturated with a carboxyl group (BG-D-COOH).

For the BG-O and BG-OH systems, the epoxy and OH groups on the basal surface strip away when the  $\text{VO}^{2+}$  approaches the surface (fig. 3 b, c). It indicates that the epoxy group and OH group on the basal surface is unstable, while the O, OH, and COOH formed on the basal plane's defects are stable and show enhanced interaction with the  $\text{VO}^{2+}$  molecule. This observation is consistent with experimental observation and will be discussed in the next sections [37]. The COOH and C=O groups in the basal plane defects showed maximum interaction with the graphite. The adsorption energies of  $\text{VO}^{2+}$  on different oxygenic groups are in the following order:

$$\text{BG-D} (-3.273 \text{ eV}) > \text{C=O} (-2.696 \text{ eV}) > \text{-COOH} (-2.538 \text{ eV}) > \text{C-H} (-1.758) > \text{-OH} (-1.35 \text{ eV}) > \text{BG} (-1.317 \text{ eV})$$

### 3.2 Interaction of the $\text{V(V)}$ with activated electrode surfaces

The adsorption of the  $\text{VO}_2^+$  on modified surfaces is investigated in a similar way as in the case of  $\text{VO}^{2+}$ . For every reference geometry, three calculations are performed, starting with three different orientations of  $\text{VO}_2^+$  (fig 2). The adsorption energies are summarised in table 2, and the most stable structures are shown in fig. 4

	<b>BG</b> (eV)	<b>BG- OH</b> (eV)	<b>BG-epoxy</b> (eV)	<b>BG-D-H</b> (eV)	<b>BG-D</b> (eV)	<b>BG-D-OH</b> (eV)	<b>BG-D-O</b> (eV)	<b>BG-D-COOH</b> (eV)
Orientation 1	-1.043	unstable	unstable	-1.396	-2.713	-0.894	-2.286	-2.12
Orientation 2	-1.066			-1.408	-2.689	-1.012	-2.321	-1.961
Orientation 3	-1.112			-1.339	-3.29	-1.144	-2.29	-2.13
<b>Most stable</b>	<b>-1.112</b>			<b>-1.408</b>	<b>-3.29</b>	<b>-1.144</b>	<b>-2.321</b>	<b>-2.13</b>

Table 2 Adsorption energies (eV) of  $\text{VO}_2^+$  at different representative geometries

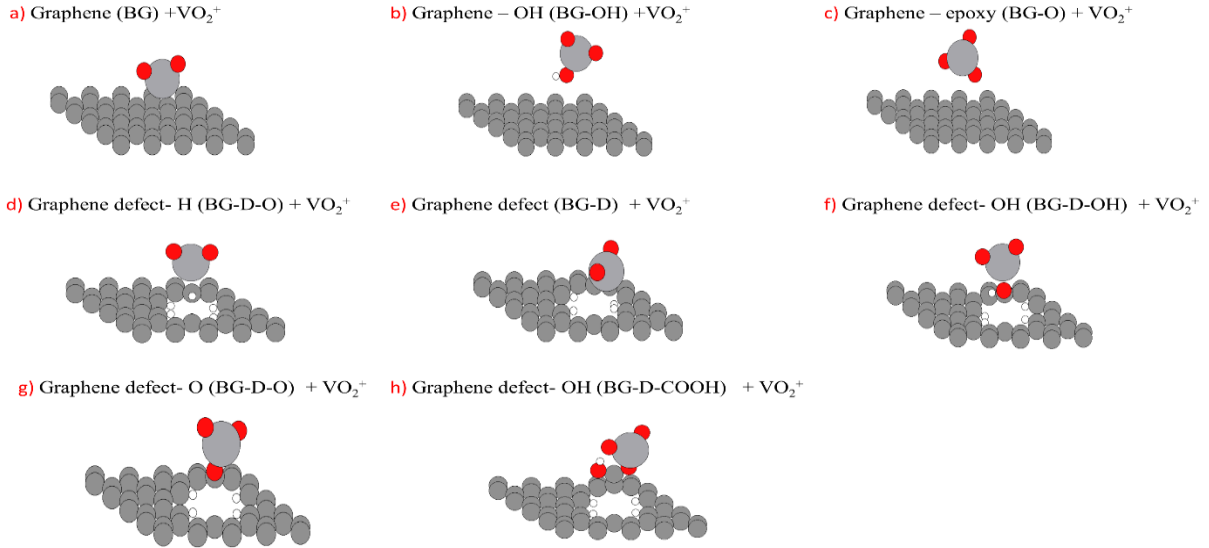


**Fig. 4** Relaxed structures of  $VO_2^+$  adsorbed on a) basal surface (BG) b) basal surface with a hydroxyl group (BG-OH), c) basal surface with epoxy group (BG-O), d) basal defect saturated with hydrogen (BG-D-H), e) basal defect (BG-D), f) basal defect saturated with a hydroxyl group (BG-D-OH), g) basal defect saturated with a carbonyl group (BG-D-O), h) basal defect saturated with a carboxyl group (BG-D-COOH).

The adsorption energy trends of  $VO_2^+$  on different functional surfaces are quite similar as in the case of  $VO^{2+}$ . The adsorption energies in Table 2 show that  $VO_2^+$  adsorbs stronger on surfaces containing functional groups on their basal plane defects. Among those, the COOH and C=O groups show the maximum affinity towards the  $VO_2^+$ , and their respective adsorption energies are 2.13 eV and 2.3 eV. The descending order of adsorption energies of the  $VO_2^+$  on all the surfaces follows:

$$BG-D (-3.29 \text{ eV}) > C=O (-2.321 \text{ eV}) > -COOH (-2.13 \text{ eV}) > C-H (-1.408) > -OH (-1.144 \text{ eV}) > BG (-1.112 \text{ eV})$$

The order of adsorption energies of the  $VO_2^+$  against different functional groups has a similar trend as for  $VO^{2+}$ . We conclude that a basal plane defect covered with functional groups has more affinity than the bare surface.

### ***3.3 Interaction of H<sub>2</sub>O with activated electrode surfaces.***

In the previous sections, the adsorption energies of VO<sup>2+</sup> and VO<sub>2</sub><sup>+</sup> are calculated on the graphite surface in vacuum. In real conditions, vanadium species are present in a solvent, mostly 3 M- 5 M H<sub>2</sub>SO<sub>4</sub> solution in water. Therefore, it is important to investigate the interaction of H<sub>2</sub>O with the graphite surface. Intrinsically, GF is hydrophobic and it requires activation to have stronger interactions with solvent [38]. In this section, the affinity of water is calculated for several representative geometries. The adsorption energies are larger when the functional groups are present on the basal defects. Among all, the -COOH group is showing maximum adsorption energy i-e -0.375 eV (table 3). The final structures are shown in fig. 5

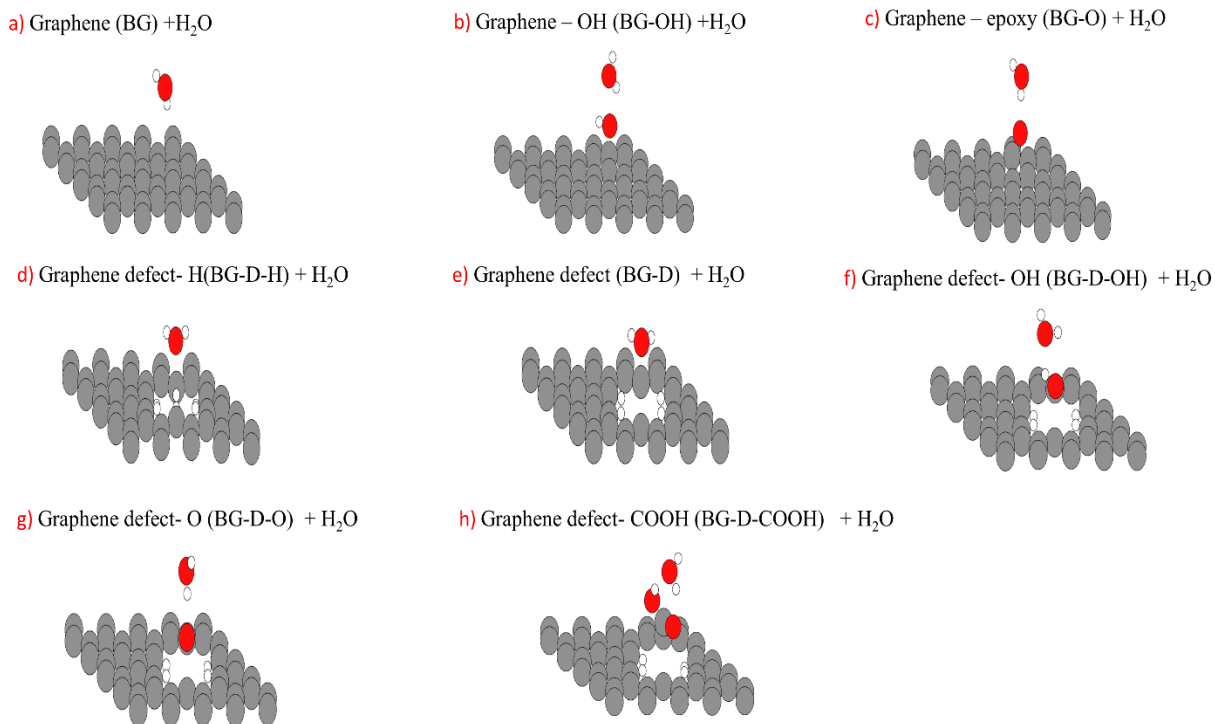


**Fig. 5** Relaxed structures of  $H_2O$  adsorbed on a) basal surface (BG) b) basal surface with a hydroxyl group (BG-OH), c) basal surface with epoxy group (BG-O), d) basal defect saturated with hydrogen (BG-D-H), e) basal defect (BG-D), f) basal defect saturated with a hydroxyl group (BG-D-OH), g) basal defect saturated with a carbonyl group (BG-D-O), h) basal defect saturated with a carboxyl group (BG-D-COOH).

	BG (eV)	BG -OH (eV)	BG-epoxy (eV)	BG-D-H (eV)	BG-D (eV)	BG-D-OH (eV)	BG-D-O (eV)	BG-D-COOH (eV)
Orientation 1	-0.1	-0.169	-0.082	-0.25	-0.287	-0.194	0.069	-0.265
Orientation 2	-0.172	-0.148	-0.099	-0.196	-0.244	-0.169	-0.199	-0.357
Orientation 3	-0.175	-0.155	-0.148	-0.159	-0.278	-0.159	-0.186	-0.305
<b>Most stable</b>	<b>-0.175</b>	<b>-0.169</b>	<b>-0.148</b>	<b>-0.25</b>	<b>-0.287</b>	<b>-0.194</b>	<b>-0.199</b>	<b>-0.357</b>

Table 3 Adsorption energies (eV) of  $H_2O$  at different representative geometries

#### 4.4 Correlation between $sp^3$ hybridization and adsorption strength on activated surfaces.

As discussed above, all the oxidative activation procedures for the carbon-based electrodes simultaneously increase the number of  $sp^3$  carbon atoms and oxygenic groups. Therefore, it is experimentally difficult to establish their individual contribution in the positive half-cell reaction's kinetics. The projected density of state (PDOS) calculations are performed and their spectra compared in fig. 6 to establish the interrelation between different oxygenic groups, surface morphology, and their affinity with the electrode.

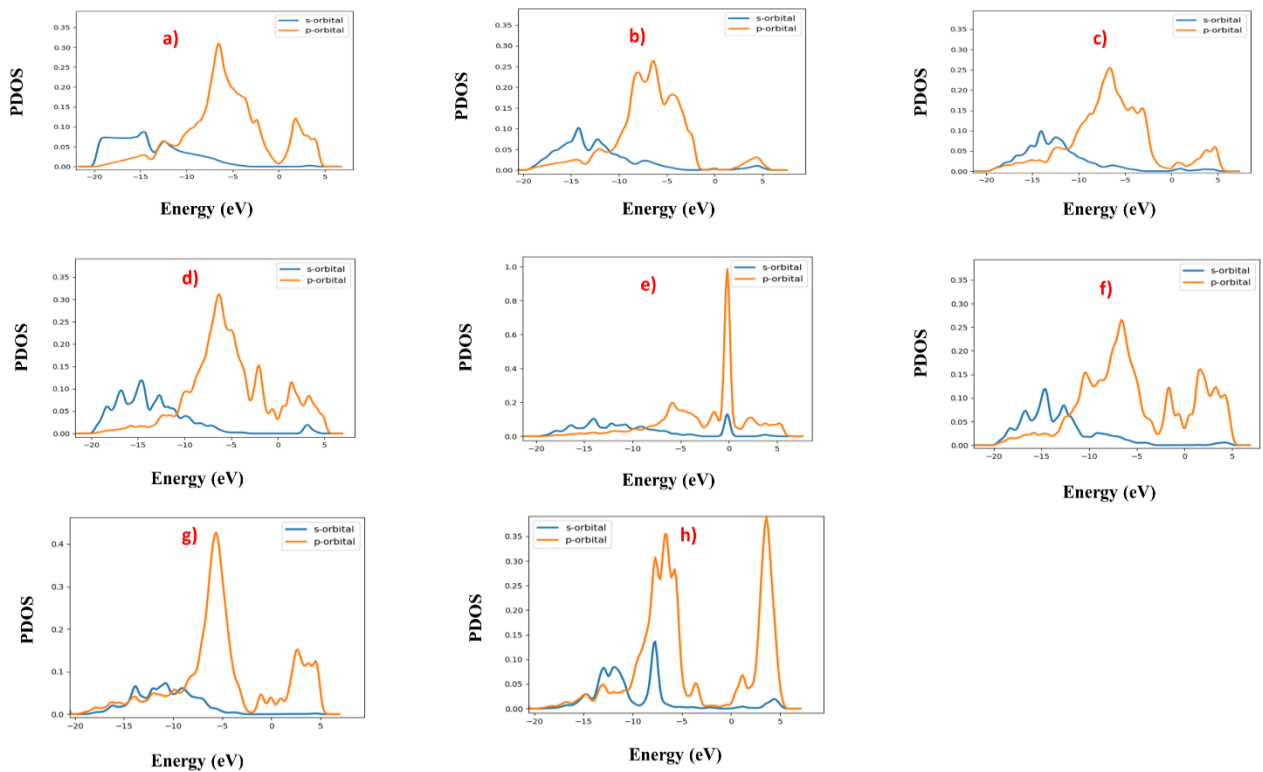


**Fig. 6** Projected density of state (PDOS) graphs of a) basal surface (BG) b) basal surface with a hydroxyl group (BG-OH), c) basal surface with epoxy group (BG-O), d) basal defect saturated with hydrogen (BG-D-H), e) basal defect (BG-D), f) basal defect saturated with a hydroxyl group (BG-D-OH), g) basal defect saturated with a carbonyl group (BG-D-O), h) basal defect saturated with a carboxyl group (BG-D-COOH).

In the calculations, the densities of states projected on the s and p orbitals are calculated. The projected density of states measures the relative probability of an electron to be present in the

different atomic orbitals at each energy. It means that the extent of the overlapping of s-orbital and p-orbital spectra in the PDOS graph shows the hybridization of s and p orbitals. Therefore, the increase of the overlap can be directly linked to the increase in  $sp^3$  hybridization. [39].

In previous sections, it is discussed that the adsorption energies of  $VO^{2+}/VO_2^+$  are greater on electrodes having oxygenic groups than on the unmodified electrode surface. The PDOS spectra of the electrode can give insights into the stronger adsorption of vanadium ions. Qualitative analysis of the PDOS spectra of BG-D-COOH (fig. 6h) and BG-D-O (fig. 6g) indicates that s and p spectra are overlapping with each other in the energy range of -20 eV to -10 eV, but there is not any overlapping observed in the case of unmodified electrode BG (fig 6a).

The overlap is quantified by integrating the s and p spectra separately over the energy range of -20 eV to -10 eV to obtain the area under curve of s and p spectra, and subsequently dividing the area of p-spectra by the area of s-spectra. The evolution of the s-p hybridization and corresponding interaction with the  $VO^{2+}/VO_2^+$  is summarized in Table 4. It is evident from the table that the adsorption energies of  $VO^{2+}$  and  $VO_2^+$  increased with the increase of the s-p hybridization. For instance,  $VO^{2+}/VO_2^+$  showed almost double adsorption energy on the electrode with the carboxylic group (BG-D-COOH) compared to the BG-D-OH. The following difference is present in s-p hybridization of both electrodes: BG-D-COOH s = 57 % p = 43 % vs BG-D-OH s = 70.6 % p = 29.4 %. Similarly, the s-p hybridization of the BG-D-O (s = 55.4 %, p= 44.6 %) is more pronounced than that of BG-D-COOH; consequently, the increase in the adsorption energy on the BG-D-O is more pronounced.

	<b>BG</b>	<b>BG-D-OH</b>	<b>BG-D-COOH</b>	<b>BG-D-O</b>
s-p spectra proportions	s = 74.5 % p = 25.5 %	s = 70.6 % p = 29.4 %	s = 57 % p = 43 %	s = 55.4 % p = 44.6 %
VO <sup>2+</sup> adsorption energy (eV)	-1.31	1.35	-2.53	-2.69
VO <sub>2</sub> <sup>+</sup> adsorption energy(eV)	-1.11	-1.14	-2.13	-2.32

**Table 4.** The percentage s and p contributions for BG, BG-D-OH, BG-D-COOH, BG-D-O, and respective VO<sup>2+</sup>/VO<sub>2</sub><sup>+</sup> adsorption energies.

It is important to note that the adsorption energies of VO<sup>2+</sup> and VO<sub>2</sub><sup>+</sup> are maximum on the BG-D. Its PDOS spectrum (fig 6e) shows a large peak around 0 eV, revealing the dangling and unstable bond nature. This bond is very reactive, and hence showing the maximum adsorption energy towards vanadium species. In reality, these dangling bonds are most likely covered with other oxygenic groups when they are introduced into the acidic electrolyte [21]. Even then, to study the interaction between the defect and vanadium ions is of theoretical interest because under VRFB's operating conditions, especially at a higher state of charge, excessive oxidation could happen, leading to the formation of CO or CO<sub>2</sub> and leaving defects behind [40,41].

To summarize the discussion, it is evident that the extent of the s-p mixing caused by the basal defects covered by the oxygenic groups follows the sequence: C=O > -COOH> -C-OH > basal surface. The binding of vanadium redox couples to the oxygenic groups follows exactly the same order. The conclusion could be drawn that the sp<sup>2</sup>/sp<sup>3</sup> hybridization is directly linked with the affinity of the positive half-cell redox couple (VO<sup>2+</sup>/VO<sub>2</sub><sup>+</sup>) with the graphite electrode, which results in higher currents and lower overpotential.[36] The fabrication of the oxygenic groups (OH, C=O, COOH) is responsible for the sp<sup>3</sup> hybridization of the carbon atoms in graphite felts.

Based on these observations, it is evident that the electrode structure is the predominant factor in the kinetics of positive half-cell reaction, which is an indirect effect of the presence of oxygenic groups. This observation is also in line with the experimental studies [16]. This insight could be very useful for materials modelling and engineering of the electrodes for the positive half-cell electrode

## 5 Conclusion

In this study, the individual roles of the different oxygenic groups and  $sp^3$  hybridization in the positive half-cell reaction of vanadium redox flow couple ( $VO^{2+}/VO_2^+$ ) are assessed via DFT calculations. Different oxygenic groups show the catalyzing effect for the  $VO^{2+}/VO_2^+$  redox couple on the graphite surface in the following order:  $C=O > COOH, > OH > \text{basal surface}$ . Projected density of states calculations show that these groups are responsible for the increase in the  $sp^3$  hybridization, and their contribution toward the increment of the  $sp^3$  hybridization is also in the same following order ( $C=O > COOH > OH$ ). The conclusion could be drawn that the increase in the  $sp^3$  hybridization is responsible for accelerating the  $VO^{2+}/VO_2^+$  reaction. Oxygenic groups are responsible for this increase. Based on this observation, some principles for the design of carbon-based VRFB electrodes can be deduced.

- The electrodes with higher  $sp^3$  hybridization should be used for the vanadium flow battery.
- The non-oxidative activation procedures should also be explored to maximize the  $sp^2/sp^3$  surface morphological changes along with more common oxidative electrode activation approaches.

- If an oxidative activation approach is used, the method's parameters should be designed to fabricate more COOH and C=O groups on the surface because they maximize the hybridization on the surface.

## Bibliography

- [1] C.Y.S. Moyeme, R.E. Hage, A. Hassan, F. Chauvet, L. Cassayre, B. Biscans, D. Quaranta, T. Tzedakis, Effect of the presence of solid particles, on the vanadyl sulfate (VOSO<sub>4</sub>) oxidation current, *Electrochim. Acta.* 373 (2021). doi:10.1016/j.electacta.2021.137909.
- [2] A.Z. Weber, M.M. Mench, J.P. Meyers, P.N. Ross, J.T. Gostick, Q. Liu, Redox flow batteries: A review, *J. Appl. Electrochem.* 41 (2011) 1137–1164. doi:10.1007/s10800-011-0348-2.
- [3] M. Zhang, M. Moore, J.S. Watson, T.A. Zawodzinski, R.M. Counce, Capital Cost Sensitivity Analysis of an All-Vanadium Redox-Flow Battery, *J. Electrochem. Soc.* 159 (2012) A1183–A1188. doi:10.1149/2.041208jes.
- [4] K.J. Kim, M.-S. Park, Y.-J. Kim, J.H. Kim, S.X. Dou, M. Skyllas-Kazacos, A technology review of electrodes and reaction mechanisms in vanadium redox flow batteries, *J. Mater. Chem. A.* 3 (2015) 16913–16933. doi:10.1039/C5TA02613J.
- [5] R. Schweiss, T. Oelsner, F. Dörfler, A. Davydov, S. Wöhner, A. Hirschvogel, Recent Insights into Carbon Felt Electrodes for Redox Flow Batteries, 2011.
- [6] K.J. Kim, S.W. Lee, T. Yim, J.G. Kim, J.W. Choi, J.H. Kim, M.S. Park, Y.J. Kim, A new strategy for integrating abundant oxygen functional groups into carbon felt electrode for vanadium redox flow batteries, *Sci. Rep.* 4 (2014) 1–6. doi:10.1038/srep06906.
- [7] M.H. Chakrabarti, R.A.W. Dryfe, E.P.L. Roberts, Evaluation of electrolytes for redox flow battery applications, *Electrochim. Acta.* 52 (2007) 2189–2195. doi:10.1016/j.electacta.2006.08.052.
- [8] M. Gattrell, J. Park, B. MacDougall, J. Apte, S. McCarthy, C.W. Wu, Study of the

- Mechanism of the Vanadium 4<sup>+</sup>/5<sup>+</sup> Redox Reaction in Acidic Solutions, *J. Electrochem. Soc.* 151 (2004) A123. doi:10.1149/1.1630594.
- [9] Z. He, Y. Jiang, H. Zhou, G. Cheng, W. Meng, L. Wang, L. Dai, Graphite felt electrode modified by square wave potential pulse for vanadium redox flow battery, *Int. J. Energy Res.* 41 (2017) 439–447. doi:10.1002/er.3626.
- [10] Y.C. Chang, J.Y. Chen, D.M. Kabtamu, G.Y. Lin, N.Y. Hsu, Y.S. Chou, H.J. Wei, C.H. Wang, High efficiency of CO<sub>2</sub>-activated graphite felt as electrode for vanadium redox flow battery application, *J. Power Sources.* 364 (2017) 1–8. doi:10.1016/j.jpowsour.2017.07.103.
- [11] Z. He, Y. Jiang, W. Meng, F. Jiang, H. Zhou, Y. Li, J. Zhu, L. Wang, L. Dai, HF/H<sub>2</sub>O<sub>2</sub> treated graphite felt as the positive electrode for vanadium redox flow battery, *Appl. Surf. Sci.* 423 (2017) 111–118. doi:10.1016/j.apsusc.2017.06.154.
- [12] L. Yue, W. Li, F. Sun, L. Zhao, L. Xing, Highly hydroxylated carbon fibres as electrode materials of all-vanadium redox flow battery, *Carbon N. Y.* 48 (2010) 3079–3090. doi:10.1016/j.carbon.2010.04.044.
- [13] K. V. Greco, A. Forner-Cuenca, A. Mularczyk, J. Eller, F.R. Brushett, Elucidating the Nuanced Effects of Thermal Pretreatment on Carbon Paper Electrodes for Vanadium Redox Flow Batteries, *ACS Appl. Mater. Interfaces.* 10 (2018) 44430–44442. doi:10.1021/acsami.8b15793.
- [14] S.M. Taylor, A. Patru, D. Perego, E. Fabbri, T.J. Schmidt, Influence of Carbon Material Properties on Activity and Stability of the Negative Electrode in Vanadium Redox Flow Batteries: A Model Electrode Study, *ACS Appl. Energy Mater.* 1 (2018) 1166–1174. doi:10.1021/acsaem.7b00273.
- [15] H. Fink, J. Friedl, U. Stimming, Composition of the Electrode Determines Which Half-Cell's Rate Constant is Higher in a Vanadium Flow Battery, *J. Phys. Chem. C.* 120 (2016) 15893–15901. doi:10.1021/acs.jpcc.5b12098.
- [16] L. Estevez, D. Reed, Z. Nie, A.M. Schwarz, M.I. Nandasiri, J.P. Kizewski, W. Wang, E.

- Thomsen, J. Liu, J.G. Zhang, V. Sprenkle, B. Li, Tunable Oxygen Functional Groups as Electrocatalysts on Graphite Felt Surfaces for All-Vanadium Flow Batteries, *ChemSusChem*. 9 (2016) 1455–1461. doi:10.1002/cssc.201600198.
- [17] B. Sun, M. Skyllas-Kazakos, Chemical modification and electrochemical behaviour of graphite fibre in acidic vanadium solution, *Electrochim. Acta*. 36 (1991) 513–517. doi:10.1016/0013-4686(91)85135-T.
- [18] A. Di Blasi, O. Di Blasi, N. Briguglio, A.S. Aricò, D. Sebastián, M.J. Lázaro, G. Monforte, V. Antonucci, Investigation of several graphite-based electrodes for vanadium redox flow cell, *J. Power Sources*. 227 (2013) 15–23. doi:10.1016/j.jpowsour.2012.10.098.
- [19] L. Zeng, T. Zhao, L. Wei, Revealing the Performance Enhancement of Oxygenated Carbonaceous Materials for Vanadium Redox Flow Batteries: Functional Groups or Specific Surface Area?, *Adv. Sustain. Syst.* 2 (2018) 1700148. doi:https://doi.org/10.1002/adsu.201700148.
- [20] Z. Jiang, K. Klyukin, V. Alexandrov, First-principles study of adsorption-desorption kinetics of aqueous  $V^{2+}/V^{3+}$  redox species on graphite in a vanadium redox flow battery, *Phys. Chem. Chem. Phys.* 19 (2017) 14897–14901. doi:10.1039/c7cp02350b.
- [21] Z. Jiang, K. Klyukin, V. Alexandrov, Ab Initio Metadynamics Study of the  $VO^{2+}/VO^{3+}$  Redox Reaction Mechanism at the Graphite Edge/Water Interface, *ACS Appl. Mater. Interfaces*. 10 (2018) 20621–20626. doi:10.1021/acsami.8b05864.
- [22] M. Meskinfam Langroudi, C.S. Pomelli, R. Giglioli, C. Chiappe, M. Aysla Costa de Oliveira, B. Mecheri, S. Licoccia, A. D'Epifanio, Interaction of vanadium species with a functionalized graphite electrode: A combined theoretical and experimental study for flow battery applications, *J. Power Sources*. 420 (2019) 134–142. doi:10.1016/j.jpowsour.2019.02.083.
- [23] A. Xu, L. Shi, L. Zeng, T.S. Zhao, First-principle investigations of nitrogen-, boron-, phosphorus-doped graphite electrodes for vanadium redox flow batteries, *Electrochim. Acta*. 300 (2019) 389–395. doi:10.1016/j.electacta.2019.01.109.

- [24] J. Enkovaara, C. Rostgaard, J.J. Mortensen, J. Chen, M. Dułak, L. Ferrighi, J. Gavnholt, C. Glinsvad, V. Haikola, H.A. Hansen, H.H. Kristoffersen, M. Kuisma, A.H. Larsen, L. Lehtovaara, M. Ljungberg, O. Lopez-Acevedo, P.G. Moses, J. Ojanen, T. Olsen, V. Petzold, N.A. Romero, J. Stausholm-Møller, M. Strange, G.A. Tritsarlis, M. Vanin, M. Walter, B. Hammer, H. Häkkinen, G.K.H. Madsen, R.M. Nieminen, J.K. Nørskov, M. Puska, T.T. Rantala, J. Schiøtz, K.S. Thygesen, K.W. Jacobsen, Electronic structure calculations with GPAW: a real-space implementation of the projector augmented-wave method, *J. Phys. Condens. Matter.* 22 (2010) 253202. doi:10.1088/0953-8984/22/25/253202.
- [25] P.E. Blöchl, Projector augmented-wave method, *Phys. Rev. B.* 50 (1994) 17953–17979. doi:10.1103/PhysRevB.50.17953.
- [26] P.E. Blöchl, C.J. Först, J. Schimpl, Projector augmented wave method:ab initio molecular dynamics with full wave functions, *Bull. Mater. Sci.* 26 (2003) 33–41. doi:10.1007/BF02712785.
- [27] A. Hjorth Larsen, J. Jørgen Mortensen, J. Blomqvist, I.E. Castelli, R. Christensen, M. Dułak, J. Friis, M.N. Groves, B. Hammer, C. Hargus, E.D. Hermes, P.C. Jennings, P. Bjerre Jensen, J. Kermode, J.R. Kitchin, E. Leonhard Kolsbjerg, J. Kubal, K. Kaasbjerg, S. Lysgaard, J. Bergmann Maronsson, T. Maxson, T. Olsen, L. Pastewka, A. Peterson, C. Rostgaard, J. Schiøtz, O. Schütt, M. Strange, K.S. Thygesen, T. Vegge, L. Vilhelmsen, M. Walter, Z. Zeng, K.W. Jacobsen, The atomic simulation environment - A Python library for working with atoms, *J. Phys. Condens. Matter.* 29 (2017). doi:10.1088/1361-648X/aa680e.
- [28] K.W. Jacobsen, Bayesian Error Estimation Functionals, in: *APS March Meet. Abstr.*, 2016: p. L31.006.
- [29] W. Li, M. Zhao, X. Zhao, Y. Xia, Y. Mu, Hydrogen saturation stabilizes vacancy-induced ferromagnetic ordering in graphene, *Phys. Chem. Chem. Phys.* 12 (2010) 13699–13706. doi:10.1039/c003524f.
- [30] B. Sun, M. Skyllas-Kazacos, Modification of graphite electrode materials for vanadium

- redox flow battery application—I. Thermal treatment, *Electrochim. Acta.* 37 (1992) 1253–1260. doi:10.1016/0013-4686(92)85064-R.
- [31] Z. Zhang, J. Xi, H. Zhou, X. Qiu, KOH etched graphite felt with improved wettability and activity for vanadium flow batteries, *Electrochim. Acta.* 218 (2016) 15–23. doi:10.1016/j.electacta.2016.09.099.
- [32] W. Zhang, J. Xi, Z. Li, H. Zhou, L. Liu, Z. Wu, X. Qiu, Electrochemical activation of graphite felt electrode for  $\text{VO}_2^+/\text{VO}_2$  redox couple application, *Electrochim. Acta.* 89 (2013) 429–435. doi:10.1016/j.electacta.2012.11.072.
- [33] S. Hariharan, M. Majumder, R. Edel, T. Grabnic, S.J. Sibener, W.L. Hase, Exploratory Direct Dynamics Simulations of  $3\text{O}_2$  Reaction with Graphene at High Temperatures, *J. Phys. Chem. C.* 122 (2018) 29368–29379. doi:10.1021/acs.jpcc.8b10146.
- [34] M. Králík, Adsorption, chemisorption, and catalysis, *Chem. Pap.* 68 (2014) 1625–1638. doi:10.2478/s11696-014-0624-9.
- [35] Y. Wan, J. Wang, F. Huang, Y. Xue, N. Cai, J. Liu, W. Chen, F. Yu, Synergistic effect of adsorption coupled with catalysis based on graphene-supported MOF hybrid aerogel for promoted removal of dyes, *RSC Adv.* 8 (2018) 34552–34559. doi:10.1039/C8RA05873C.
- [36] A. Hassan, T. Tzedakis, Enhancement of the electrochemical activity of a commercial graphite felt for vanadium redox flow battery (VRFB), by chemical treatment with acidic solution of  $\text{K}_2\text{Cr}_2\text{O}_7$ , *J. Energy Storage.* 26 (2019) 100967. doi:10.1016/j.est.2019.100967.
- [37] G. Wei, W. Su, Z. Wei, X. Fan, J. Liu, C. Yan, Electrocatalytic effect of the edge planes sites at graphite electrode on the vanadium redox couples, *Electrochim. Acta.* 204 (2016) 263–269. doi:10.1016/j.electacta.2016.04.081.
- [38] A. Hassan, T. Tzedakis, Facile chemical activation of graphite felt by  $\text{KMnO}_4$  acidic solution for vanadium redox flow batteries, *Appl. Surf. Sci.* 528 (2020) 146808. doi:10.1016/j.apsusc.2020.146808.
- [39] S. Yadav, J. Tam, C.V. Singh, A first principles study of hydrogen storage on lithium

decorated two dimensional carbon allotropes, *Int. J. Hydrogen Energy*. 40 (2015) 6128–6136. doi:10.1016/j.ijhydene.2015.03.038.

- [40] F. Mohammadi, P. Timbrell, S. Zhong, C. Padeste, M. Skyllas-Kazacos, Overcharge in the vanadium redox battery and changes in electrical resistivity and surface functionality of graphite-felt electrodes, *J. Power Sources*. 52 (1994) 61–68. doi:10.1016/0378-7753(94)01938-X.
- [41] B. Sun, M. Skyllas-Kazacos, Chemical modification of graphite electrode materials for vanadium redox flow battery application-part II. Acid treatments, *Electrochim. Acta*. 37 (1992) 2459–2465. doi:10.1016/0013-4686(92)87084-D.